PET and Parathyroid L-[Carbon-11]Methionine Accumulation in Hyperparathyroidism

Anders Sundin, Claes Johansson, Per Hellman, Mats Bergström, Håkan Ahlström, Gunilla B. Jacobson, Bengt Långström and Jonas Rastad

Departments of Diagnostic Radiology and Surgery, and Uppsala University PET Center, Uppsala, Sweden

The study was designed to characterize L-[methyl-^{11}C]methionine accumulation in abnormal parathyroid tissues of hyperparathyroidism (HPT). **Methods:** Thirty-four patients with primary (n = 32) or secondary HPT were investigated with PET before primary or reoperative (n = 25) parathyroid surgery. Parathyroid ^{11}C-methionine accumulation was analyzed for integrated uptake values in defined tissue volumes standardized for the injected dose and body weight (SUV), four contiguous pixels of maximal accumulation (SUV_{hs}), SUV multiplied by area of region of interest (SUV_r) and by the excised tissue weight (SUV_w). Transport rate constants (slope, $slope_{hs}$) were calculated according to Patlak's formula using plasma ^{11}C activity corrected for ^{11}C-methionine metabolites. **Results:** True-positive localization was achieved in 85% of patients in whom 81% of the excised parathyroid lesions were visualized; no false-positive results were obtained. Corresponding proportions were 59% and 57% for CT and 55% and 52% for ultrasound, respectively. In the true-positive cases, parathyroid SUV, SUV_{hs} and transport rate constants were consistently higher ($p < 0.01$) than in the thyroid, pharynx-esophagus, neck muscle and apical lung. Parathyroid SUV, SUV_{hs} and SUV_r increased with intact serum parathyroid hormone and calcium values (p = 0.0001–0.031), and weight of the excised tissue correlated with SUV and SUV_{hs} (p = 0.024, 0.044). Parathyroid SUV_{hs} varied strongly with the transport rate constants (p = 0.0008), and SUV_r as well as s-calcium values differed significantly between parathyroid adenomas (n = 11), chief cell hyperplasias (n = 13), inadvertent implants (n = 3) and parathyroid cancers (n = 3). **Conclusion:** Carbon-11-methionine PET has potential application in preoperative localization and metabolic characterization of abnormal parathyroid tissues in human HPT.

Key Words:. PET; carbon-11-methionine; parathyroid gland; hyperparathyroidism

J Nucl Med 1996; 37:1766–1770

Pathological parathyroid tissue of patients with hyperparathyroidism (HPT) is characterized by increased secretion of parathyroid hormone (PTH) in relation to the serum calcium level. The severity of this rise determines the degree of hypercalcemia and relates to derangements in calcium sensitivity of the hormone release (*1,2*). The secretory control of extracellular calcium has been attributed to calcium-sensing receptors on the surface of the parathyroid cells (*3,4*). Such a 500-kDa protein exhibits decreased expression and possibly fails to adequately suppress the hormone release in HPT, irrespective of this disorder being primary or secondary, adenomatous, hyperplastic or malignant in character (*2,5*). HPT invariably is also associated with increased parathyroid cell mass, which might contribute to elevated PTH levels (*2,6*). The rate of cell proliferation is usually meager and might vary with time in pathological parathyroid tissue (*7,8*).

An earlier PET study (*9*) supported the view that abnormal human parathyroid tissue of HPT expressed substantial accumulation of ^{11}C-methionine, which enabled efficient preoperative localization of even the less conspicuously enlarged glands. The current study evaluates an extended material of patients with mainly postoperatively persistent or recurrent HPT for the efficiency of ^{11}C-methionine PET in parathyroid gland localization and for hitherto unexplored characteristics in vivo of ^{11}C-methionine accumulation in different types of the abnormal human parathyroid tissues.

MATERIALS AND METHODS

We studied 34 hypercalcemic patients with HPT (26 women, 8 men; age 33–80 yr; mean age 61 yr). They were scheduled for surgery due to sporadic primary HPT (n = 25), HPT of multiple endocrine neoplasia (MEN) type 1 (n = 7) or chronic renal insufficiency (n = 2). Recruitment into the study consecutively encompassed those fulfilling indications for parathyroid re-exploration (n = 25) due to persistence or recurrence of HPT. These patients had undergone 1–4 parathyroid or thyroid operations involving bilateral exploration of the neck. Those investigated before primary operation (n = 9) were included in the series mainly to disclose the approximate glandular mass required for positive localization. At the time of the PET investigation, the patients exhibited albumin-corrected total serum (s) calcium of 2.66–3.30 mmol/liter and intact s-PTH of 36–520 ng/liter (Table 1). The individuals with uremic HPT had undergone kidney transplantation and demonstrated satisfactory renal function (average s-creatinine, 104 μmol/liter; reference range, 64–106 μmole/liter). The patients gave informed consent to participate in the study, which was approved by the local Ethics and Isotope Committees.

Parathyroid surgery was performed 0.5–9.2 mo (mean, 1.3 mo) after the PET investigation. All specimens were weighed and subjected to conventional histopathological examination (*10*). All total, 37 abnormal parathyroid tissue accumulations were excised, since 3 patients displayed pairs of abnormal glands at exploration. All the tissues were located in the neck, except in one patient with recurrent uremic HPT due to growth of a forearm autotransplant. Total wet weight of the specimens was 80 to 6,000 mg (Table 1). All total, 13 patients demonstrated parathyroid adenoma (130–6,000 mg), while hyperplasia with a total weight of 80–2000 mg was found in 14 individuals. Such hyperplasia was considered in all patients with more than a single enlarged parathyroid gland (>60 mg) and in HPT of uremia and MEN 1 (*6,10*). Parathyroid carcinoma (110–600 mg) was recognized in three patients by the unequivocal criterion of metastases, and these individuals underwent a second to fourth surgical procedure for recurrent disease. Inadvertent implants of parathyroid tissue (100–750 mg) were found in four patients who had previously undergone extirpation of parathyroid adenoma or hyperplasia of primary HPT. These implants consisted of multiple aggregations of nodularly arranged chief cells. Evaluation of the dominant type of parathyroid parenchyma confirmed that all hyperplasias and cancers were of the chief cell type. This circumstance also applied to all

Received Oct. 10, 1995; revision accepted Mar. 6, 1996.

For correspondence or reprints contact: Jonas Rastad, MD, Department of Surgery, University Hospital, S-751 85 S-751 85 Uppsala, Sweden.

TABLE 1
Mean ± s.d. for Total s-Calcium (CaT, mmol/liter), Ionized p-Calcium (Cal, mmol/liter), Intact s-PTH (ng/liter) and Total Weight (mg) of Excised Parathyroid Tissues

	CaT	Cal	PTH	Weight
Adenoma (n = 13)	2.94 ± 0.19	1.43 ± 0.10	153 ± 126	888 ± 1598
Hyperplasia*	2.79 ± 0.02	1.38 ± 0.06	68 ± 24.3	401 ± 476
Carcinoma (n = 3)	3.21 ± 0.08	nd	195 ± 18.0	370 ± 246
Implants (n = 4)	2.99 ± 0.06	1.44 ± 0.09	147 ± 53.9	435 ± 300
Total (n = 34)	2.91 ± 0.18	1.42 ± 0.09	127 ± 94	574 ± 1007

*Multiple parathyroid gland enlargement of sporadic HPT, familial and uremic HPT. nd = not done.

adenomas, except one mainly consisting of oxyphil and transitional oxyphil cells. All patients displayed normocalcemia at follow-up (0.9–2.4 yr; mean, 1.3 yr) postoperatively.

PET Imaging

Carbon-11 was produced as $^{11}CO_2$ by the $^{14}N(p, \alpha)$ ^{11}C reaction using a 17-MeV cyclotron. Carbon-11-methionine was synthesized through ^{11}C-methyl iodide and prepared for intravenous administration (*11*). After an overnight fast allowing free intake of liquids, the patients were examined in a whole-body PET camera which simultaneously produced 15 contiguous 6.5-mm axial slices with an in-plane resolution of 5–6 mm (*12*). The patients were placed supine and a laser beam was used for positioning. The axial field of view was 10 cm and included the neck and superior mediastinum. A 10-min transmission scan was generated with an external rotating ^{68}Ge pin to correct the ensuing emission scan for attenuation. After a rapid intravenous bolus of 750 ± 141 MBq (mean ± s.d.) ^{11}C-methionine, a 45-min dynamic examination sequence was started. Plasma samples from a foot vein, "arterialized" by heating, were drawn to monitor ^{11}C-methionine clearance and were measured in a well scintillation crystal detector cross-calibrated with the camera (n = 15).

Dynamic images were reconstructed in a 128 × 128 matrix with a 6-mm Hanning filter. Data obtained 15–45 min after the injection were corrected for attenuation and scattered radiation and summed to create an average image. The radioactivity concentrations in this image were recalculated to provide images of standardized uptake values (SUV), whereby the concentration in each pixel was divided by the injected dose per gram body weight. Regions of interest (ROIs) were drawn manually in the summation images to include visualized parathyroid glands in the axial image showing their greatest appreciable area, the thyroid, pharynx–esophagus, cervical vertebra, neck muscle and apical parts of the lung. These tissues were delineated by an isocontour (mean ROI), which was positioned halfway between the greatest activity in the specified tissue and its immediate surroundings (Fig. 1). Relations between total accumulated tracer in the parathyroid tissue and the biochemical parameters were explored by multiplying SUV with the mean ROI area (SUV_r) and with the weight of the extirpated parathyroid specimen (SUV_w). An additional region was drawn in each ROI, which was designated as the "hot spot" (hs) and comprised four contiguous pixels (0.64 cm^2) of the highest SUV (ROI_{hs}). Images of the transport rate into the tissues were generated on a pixel basis by using the plasma radioactivity as reference (*13*). Plasma ^{11}C activity values were corrected for ensuing ^{11}C-methionine metabolites. Due to the lack of individual analyses of plasma methionine metabolism, a standard correction was calculated from previous data (*14*). The ROIs from the SUV images were applied to the Patlak images. The transport rate constants for ROI and ROI_{hs} in the various tissues were denoted slope and $slope_{hs}$, respectively. In addition, the mass influx of ^{11}C-methionine (μmole/min × 100 ml) was calculated by multiplying the transport rate constants by the plasma concentration of "cold" methionine.

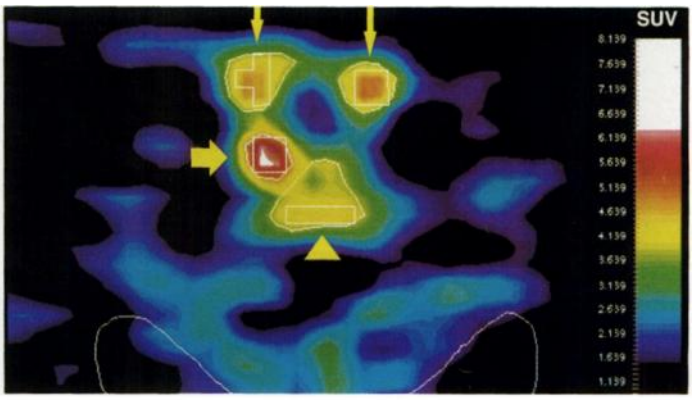

FIGURE 1. Transverse ^{11}C-methionine PET image of the neck with true-positive localization of a 400-mg parathyroid adenoma and manually applied ROIs delineating the adenoma (thick arrow), thyroid gland (thin arrows), vertebral body (arrow head) and large ROI in the posterior neck muscles.

CT and Ultrasonography

Intravenous contrast-enhanced CT was performed with a scanner using a 4-mm slice thickness and increment (n = 29). For anatomical correlation of the ^{11}C-methionine uptake, CT scans were compared with the PET images. Ultrasonography (US) utilized an apparatus equipped with a 5- or 7.5-MHz linear transducer (n = 29).

Biochemistry

Total s-calcium (reference range, 2.20–2.60 mmol/liter) was measured by an automated complexiometric orthocresolophthalein technique and invariably corrected for the concomitant s-albumin level. Ionized plasma (p) calcium values were adjusted for pH (reference range, 1.12–1.29 mmol/liter) and analyzed with an ion-selective electrode. Intact s-PTH (reference range, 12–55 ng/liter) was estimated with the Allegro Immunoradiometric assay (Nichol's Institute, San Juan, CA).

Statistical Analysis

Group means were investigated with two-tailed Student's t-test for paired (intraindividual) or unpaired data. Correlations utilized Pearson's correlation coefficients. One-way analysis of variance (ANOVA) was used to compare multiple groups. A p value of <0.05 was considered statistically significant. Values are presented as means ± s.d.

RESULTS

True-positive localization was achieved by PET in 29 patients (85%) exhibiting 30 (81%) correctly detected parathyroid lesions. The weight of the depicted lesions was 110–6,000 mg (703 ± 1,222 mg). In the first five patients of the series, however, the PET findings were equivocal and positive localization was established at re-evaluation. Two abnormal parathyroid glands were revealed by PET in one of the three patients exhibiting such enlargement, whereas the second gland (80 mg, 100 mg) was missed in the others. PET was false-negative in four patients (12%) harboring 6 undetected lesions (16%) of 80, 100, 130, 200, 400 and 750 mg. Essentially similar proportions of adenomas (85%), hyperplasias (81%), implants (75%) and cancers (100%) were localized. Since there were no false-positive results, the specificity was 100%. When only the reoperative cases were considered (n = 25), true-positive localization was achieved in 88% of the patients and for 81% of the excised glands. CT and US were true-positive in 59% and 55% of the patients, and they correctly localized 57% and 52%

TABLE 2
Mean ± s.d. for SUV, SUV_{hs}, SUV_r (cm^2), SUV_w (g), and Transport Rate Constants [Slope and $Slope_{hs}$, (/min × 10^{-2})] in Subgroups of Abnormal Parathyroid Glands and Other Tissues

Organ	SUV	SUV_{hs}	SUV_r	SUV_w	Slope	$Slope_{hs}$
Parathyroid (n = 30)	3.9 ± 1.3	4.6 ± 1.8	2.9 ± 0.2	127 ± 94	6.3 ± 2.6	7.1 ± 3.1
Adenoma (n = 11)	3.8 ± 0.4	4.9 ± 2.1	2.9 ± 0.2	153 ± 126	6.8 ± 2.9	7.7 ± 3.3
Hyperplasia (n = 13)	3.6 ± 1.3	4.2 ± 1.6	2.8 ± 0.1	68 ± 24	4.7 ± 1.4	5.3 ± 1.9
Implant (n = 3)	4.1 ± 1.4	4.5 ± 1.8	3.0 ± 0.1	147 ± 54	7.3 ± 4.4	8.3 ± 5.3
Cancer (n = 3)	5.2 ± 1.2	5.6 ± 1.1	3.2 ± 0.1	195 ± 18	5.8 ± 0.8	6.2 ± 1.2
Thyroid*	3.2 ± 0.8	3.6 ± 0.9	nd	nd	4.3 ± 1.2	4.6 ± 1.8
Vertebral body	4.3 ± 0.9	5.2 ± 1.1	nd	nd	6.9 ± 2.4	8.4 ± 3.4
Esophagus	3.1 ± 0.8	3.4 ± 0.8	nd	nd	4.7 ± 1.4	5.1 ± 1.6
Lung†	0.67 ± 0.70	nd	nd	nd	0.70 ± 0.31	nd

*Mean of both thyroid lobes except in previous hemithyroidectomies.
†Apices alone; nd = not done.

of the lesions, respectively. One lesion (4%) was false-positive with US.

The parathyroid SUV_{hs} was 22% higher than SUV, and $slope_{hs}$ exceeded the slope by 13% (Table 2). Intraindividual comparison of SUV and SUV_{hs} demonstrated 30% ($p = 0.006$) and 36% ($p = 0.0042$) higher values in the parathyroid than in the thyroid (n = 30). Comparison of the parathyroid and thyroid tissues also displayed 62% greater slope ($p = 0.0064$) and $slope_{hs}$ ($p = 0.0065$) values. Only cervical vertebrae demonstrated SUV and slope values comparable to or higher than the parathyroid glands ($p < 0.22–0.01$). In contrast, these values were significantly lower in the pharynx-esophagus, muscle and lung compared to the parathyroid ($p = 0.0001–0.0046$). The kinetics of ^{11}C-methionine accumulation were similar in parathyroid adenomas, hyperplasias and implants (Fig. 2A-C). Peak activity was reached within the minute after injection and then declined over 5 min to approximately half the peak activity. Rare parathyroid cancers demonstrated a somewhat later activity peak, and the virtually constant SUV averaged about 80% of peak activity (Fig. 2D). The pattern of thyroid uptake resembled that of the parathyroid adenomas, hyperplasias and implants, but for the generally lower SUV level (Fig. 2E).

Intact s-PTH increased with total s-calcium ($p = 0.0001$), ionized p-calcium ($p = 0.046$), and weight of the parathyroid tissue ($p = 0.0001$) in the patient sample. Both SUV and SUV_{hs} increased with parathyroid weight, s-PTH and total s-calcium (Table 3). Parathyroid SUV_r and SUV_w correlated with total s-calcium, ionized p-calcium, and s-PTH. There were no significant correlations in these respects, however, for the transport rate constants, although parathyroid SUV_{hs} correlated positively with the slope and $slope_{hs}$ ($p = 0.0008$). In the morphological subgroups of parathyroid tissues, total s-calcium and SUV_r values differed significantly ($p = 0.0001–0.0480$). Both of them were lowest in the hyperplasias, highest in the cancers and intermediate in the adenomas and implants (Table 2). The hyperplasias and implants could not be separated with respect to either of these values ($p = 0.59$). Otherwise the biochemical indices of HPT, total glandular weight and the

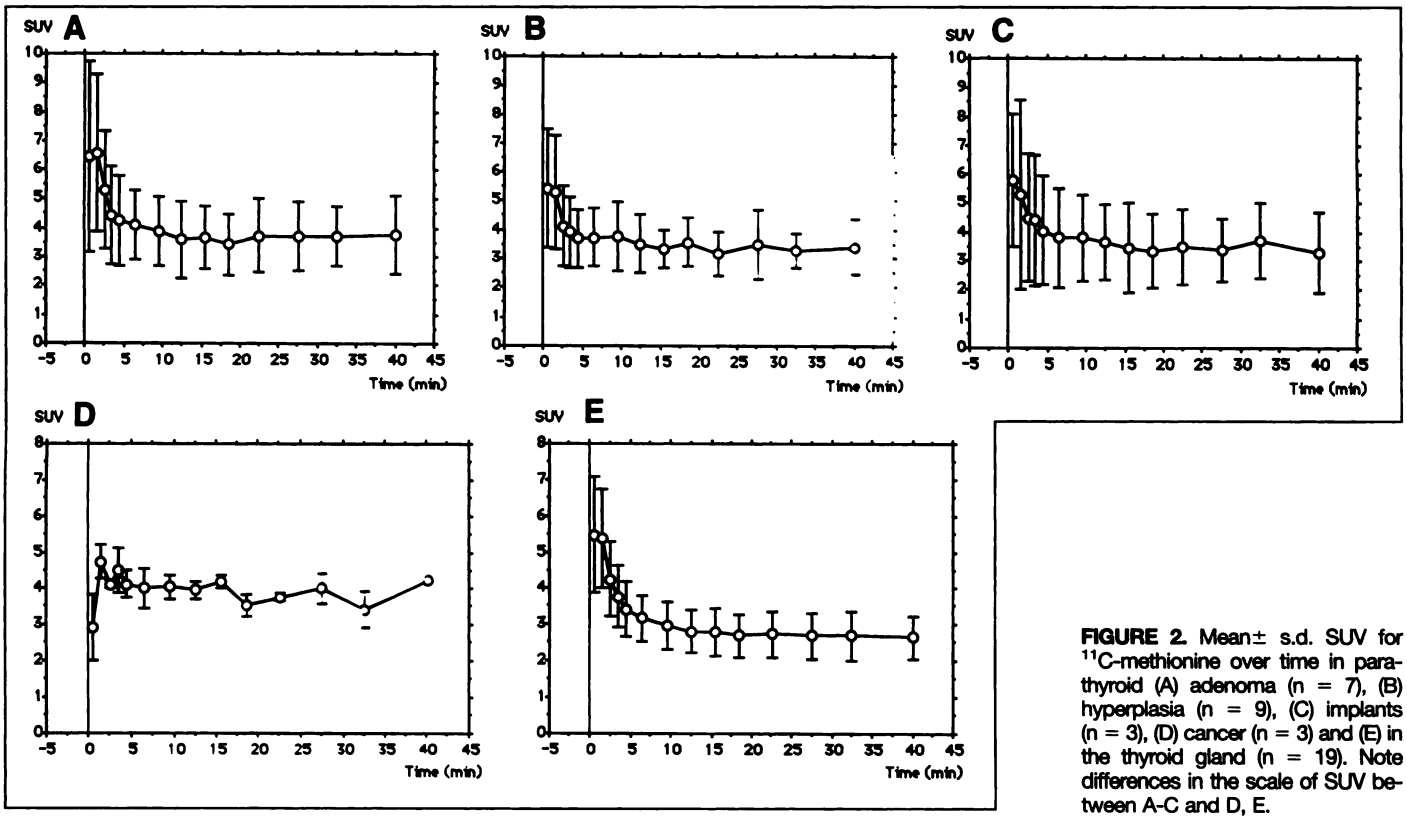

FIGURE 2. Mean± s.d. SUV for ^{11}C-methionine over time in parathyroid (A) adenoma (n = 7), (B) hyperplasia (n = 9), (C) implants (n = 3), (D) cancer (n = 3) and (E) in the thyroid gland (n = 19). Note differences in the scale of SUV between A-C and D, E.

TABLE 3
Probabilities of Correlation between Parathyroid Carbon-11-Methionine Accumulation Parameters and Indices of HPT

	SUV	SUV_{hs}	SUV_r	SUV_w	Slope	$Slope_{hs}$
s-PTH	0.013	0.016	<0.001	<0.001	ns	0.016
Total s-calcium	0.031	0.003	<0.001	<0.001	ns	0.003
Ionized p-calcium	ns	ns	0.048	0.046	ns	ns
Total weight	0.024	0.044	ns	nd	ns	0.044

ns = not significant; nd = not done.

explored characteristics of ^{11}C-methionine accumulation failed to differ significantly between the subgroups of HPT. Despite the numerically lowest mean glandular weight, however, parathyroid carcinoma displayed the highest SUV, SUV_{hs}, SUV_r, SUV_w values, while these variables were the lowest in the hyperplasias. In contrast, the implants demonstrated the greatest slope, $slope_{hs}$ and ^{11}C-methionine mass influx values.

DISCUSSION

The present patient series is extraordinary with respect to the representation of different histological entities of parathyroid disease. In comparison to generally unselected conditions, overrepresentation of parathyroid chief cell hyperplasia, carcinoma and inadvertent tissue implants were encountered (*15*). This circumstance relates mainly to the routine application of preoperative procedures of parathyroid gland localization solely in individuals undergoing parathyroid reoperation (*16*). Evaluation of ^{11}C-methionine PET demonstrated 85% true-positive localization of the abnormal parathyroid tissue in the 34 patients, and 81% of the lesions were detected. Consistent with the results in an earlier study (*9*), these findings were superior to the results of CT and US. Moreover, the difference toward CT and US persisted when the reoperative patients alone were considered. The parathyroid detection rates for CT and US in the present study generally were comparable to previous findings (*17,22*), although more efficient modalities may include ^{99m}Tc-sestamibi scintigraphy (*17,23,24*). Nevertheless two of the glands missed by PET were correctly localized by US and another one by CT, which supports the finding that these examinations are complementary to ^{11}C-methionine PET. Five glands were unequivocally positive solely at re-evaluation of the PET images. The primary viewing of these cases mainly comprised the initial learning phase for the two radiologists evaluating the images. Corresponding re-evaluation of the other patients, including all CT scans yielded no additional visualizations.

Evidently, size of the parathyroid tissues influenced glandular localization with ^{11}C-methionine PET. All but two undetected lesions weighed 80–200 mg, while the weight of positively detected glands averaged 660 ± 1120 mg. By disregarding five lesions weighing 140–180 mg, it seems reasonable to conclude that positive detection with ^{11}C-methionine PET essentially required parathyroid tissue weights exceeding about 200 mg. Moreover, a spherical 200-mg gland corresponds to a diameter of approximately 7.5 mm, a size below which resolution of the PET camera starts to limit the visibility. Moreover, the learning factor possibly explained the failure to localize three lesions weighing 180–275 mg, and that two glands weighing 750 and 940 mg were unequivocally detected only during image re-evaluation. Average uptake of ^{11}C-methionine in the abnormal parathyroid tissues exceeded that of other structures in the neck and upper thorax, except for cervical vertebrae. Only residual thyroid lobes posed problems during image interpretation, and the lesions providing false-negative or primarily equivocal interpretations were mainly juxtathyroid. Normal neck tissue uptake of ^{11}C-methionine offered excellent anatomical landmarks, which facilitated image interpretation and provided the surgeon with relevant details on glandular location. This benefit is not provided by PET with [^{18}F]FDG, the only tracer other than ^{11}C-methionine that has been evaluated in HPT. FDG has been utilized in limited series of patients subjected to primary parathyroid exploration with highly discrepant findings as regards true- and false-positive localizations (*25–27*). Previously, we have consistently failed to localize enlarged parathyroid glands with FDG-PET in reoperative patients exhibiting true-positive visualization by ^{11}C-methionine PET (unpublished data).

Downregulation of a surface calcium receptor on the abnormal parathyroid cells seems to explain the relative insensitivity of the PTH secretion to extracellular calcium and the extent of s-calcium and intact s-PTH elevations in HPT (*2,28–30*). The proliferative derangement in the pathological parathyroid tissues is less characterized (*7,31*). Since the increased parathyroid cell mass may contribute to the s-PTH elevation in HPT, biochemical indices of the parathyroid disorder in vivo may reflect interactions between the deranged cell growth and secretion. Consistent with the current findings, however, s-PTH usually correlates with both the abnormal parathyroid tissue weight and s-calcium in primary HPT (*32,33*). Accumulation of ^{11}C-methionine reflects several phenomena, including protein synthesis, transmethylation processes with methionine as methyl donor, and transmembrane amino acid transport (*34*), which were indistinguishable with the present methodology. The enhanced uptake of ^{11}C-methionine in most tumors, which forms the basis for the diagnostic potential of the tracer (*35*), cannot be attributed solely to proliferation. Secretory activity may induce appreciable increase in ^{11}C-methionine uptake (*36*), but basal protein synthesis unrelated to secretory activity should be expected to predominate in many instances (*37*).

The present findings emphasize that ^{11}C-methionine accumulation correlated to parathyroid tissue characteristics. The correlations between s-PTH, s-calcium and parathyroid SUV_{hs} corroborate observations on other hormonally active tumors and indicate that cellular methionine metabolism is activated to a greater extent in the more secretory hyperactive glands (*26,27*). Consistent with this hypothesis SUV_r and SUV_w, which include contributions from the glandular mass as well as the activity per cell, strongly correlated to the in vivo indices of HPT. Moreover, parathyroid hyperplasias generally demonstrated the lowest SUV, SUV_{hs}, transport rate constants as well as SUV_r and SUV_w in addition to intermediate mean glandular weight. Interestingly, adenomas, despite a high glandular weight, showed the greatest transport rate constants but intermediate SUV, SUV_{hs} and mass influx values. Carcinomas substantiated the highest SUV, SUV_{hs} and mass influx values and the lowest mean weight. These circumstances are consistent with the severe perturbation of this tissue, which even at a moderate cell

mass induced the highest s-calcium and PTH levels. The lack of correlation for transport rate constants and mass influx values might reflect that these parameters include estimates on plasma radioactivity and methionine levels and possibly were subjected to larger variations than SUV. Additional factors may be related to the quantification technique. An improvement in this respect could consist of an adapted image reformatting, whereby the imaged volume could be resliced in the plane of the largest visualized tissue area. Indeed, the size of all parathyroid glands permitted detection in at least two contiguous slices, and linking of ROIs to create volumes of interest may further increase the diagnostic accuracy. By disregarding the hot spot measurements, the currently acquired characteristics of parathyroid ^{11}C-methionine accumulation consequently should be considered to reflect a major portion of the analyzed glands.

CONCLUSION

The kinetics of ^{11}C-methionine uptake were similar for the thyroid and all subgroups of parathyroid tissue but carcinomas. The initial phase of ^{11}C-methionine uptake depends on blood flow, blood volume and tracer extraction. To what extent these factors differed between the carcinomas and other tissues cannot be concluded from the present data. The generally smaller vascular volume in malignant tumors than in normal tissues may at least partly explain these kinetic differences. Moreover, it remains to be established if these and other characteristics of ^{11}C-methionine accumulation may improve the difficult distinction between different subgroups of hyperparathyroid tissues (*6,10*). Conventional methods for preoperative localization, such as CT, US and scintigraphy, rely more or less exclusively on tumor size and degree of vascularization (*16*). The fact that ^{11}C-methionine PET also seems to reflect other parathyroid derangements of HPT may be clinically useful, particularly in cases where the degree of tumor tissue dysfunction and proliferation fails to aggravate in parallel. HPT of type MEN 1, and parathyroid carcinoma in particular, may be examples in this respect. Moreover, parathyroid tissue implants exhibit substantial tissue area and meager weight and have been consistently difficult to visualize preoperatively (*16*).

The current findings strongly support that ^{11}C-methionine PET should be regarded as an interesting tool in the localization and characterization of abnormal human parathyroid tissue in vivo.

REFERENCES

1. Juhlin C, Johansson H, Holmdahl R, et al. Monoclonal anti-parathyroid antibodies interfering with a Ca^{2+}-sensor of human parathyroid cells. *Biochem Biophys Res Commun* 1987;143:570–574.
2. Wallfelt C, Gylfe E, Larsson R, Ljunghall S, Rastad J, Åkerström G. Relationship between external and cytoplasmic calcium concentrations, parathyroid hormone release and weight of parathyroid glands in human hyperparathyroidism. *J Endocrinol* 1988;116:457–464.
3. Brown EM, Gamba G, Riccardi D, et al. Cloning and characterization of an extracellular Ca^{2+}-sensing receptor from bovine parathyroid. *Nature* 1993;366:575–580.
4. Lundgren S, Hjälm G, Hellman P, et al. A protein involved in calcium sensing of the human parathyroid and placental cytotrophoblast cells belongs to the LDL-receptor protein superfamily. *Exp Cell Res* 1994;212:344–350.
5. Nygren P, Gylfe E, Larsson R, et al. Modulation of the Ca^{2+}-sensing function of parathyroid cells in vitro and in hyperparathyroidism. *Biochem Biophys Acta* 1988; 968:253–260.
6. Åkerström G, Rudberg C, Grimelius L, et al. Histologic parathyroid abnormalities in an autopsy series. *Hum Pathol* 1986;17:520–527.
7. Nygren P, Larsson R, Johansson H, Ljunghall S, Rastad J, Åkerström G. $1,25(OH)_2D_3$ inhibits hormone secretion and proliferation but not functional dedifferentiation of cultured bovine parathyroid cells. *Calcif Tiss Int* 1988;43:213–218.
8. Parfitt AM, Willgoss D, Jacobi J, Lloyd HM. Cell kinetics in parathyroid adenomas: evidence for decline in rates of cell birth and tumour growth, assuming clonal origin. *Clin Endocrinol* 1991;35:151–157.
9. Hellman P, Ahlström H, Bergström M, et al. Positron emission tomography with ^{11}C-methionine in hyperparathyroidism. *Surgery* 1994;116:974–981.
10. Grimelius L, Åkerström G, Johansson H, Juhlin C, Rastad J. The parathyroid glands. In: Kovacs K, Asa L, eds. *Functional endocrine pathology.* Boston: Blackwell Scientific Publishers; 1991:375–395.
11. Långström B, Antoni G, Gullberg P, et al. Synthesis of l- and d-[methyl-^{11}C]-methionine. *J Nucl Med* 1987;28:1037–1040.
12. Kops ER, Herzog H, Schmid A, Holte S, Feinendegen LE. Performance characteristics of an eight-ring whole-body PET scanner. *J Comput Assist Tomogr* 1990;14:437–445.
13. Patlak CS, Blasberg RG, Fenstermacher JD. Graphic evaluation of blood-to-brain transfer constants from multiple-time uptake data. *J Cereb Blood Flow Metab* 1983;3:1–7.
14. Hatazawa J, Ishiwata K, Itoh M, et al. Quantitative evaluation of L-[methyl-C-11]-methionine uptake in tumor using positron emission tomography. *J Nucl Med* 1989;30:1809–1813.
15. Åkerström G, Rudberg C, Grimelius L, Johanson H, Lundström B, Rastad J. Causes of failed primary exploration and technical aspects of reoperation in primary hyperparathyroidism. *World J Surg* 1992;16:562–568.
16. Rastad J. Radiological means of parathyroid localization and ablation. In: Åkerström G, Rastad J, Juhlin C, eds. *Current controversy in parathyroid operation and reoperation.* Austin, TX: RG Landes Co.; 1994:123–149.
17. Casas AT, Burke GJ, Sathyanarayana, Mansberger A, Wei JP. Prospective comparison of technetium-99m-sestamibi/iodine-123 radionuclide scan versus high-resolution ultrasonography for the preoperative localization of abnormal parathyroid glands in patients with previously unoperated primary hyperparathyroidism. *Am J Surg* 1993; 166:369–373.
18. McIntyre R, Kumpe DA, Liechty RD. Re-exploration and angiographic ablation for hyperparathyroidism. *Arch Surg* 1994;129:499–503.
19. Thompson CT, Bowers J, Broadie TA. Preoperative ultrasound and thallium-technetium subtraction scintigraphy in localizing parathyroid lesions in patients with hyperparathyroidism. *Am Surg* 1993;59:509–511.
20. Pearl AJ, Chapnik JS, Freeman JL, et al. Preoperative localization of 25 consecutive parathyroid adenomas: a prospective imaging/surgical correlative study. *J Otolaryngol* 1993;22:301–306.
21. Erdman WA, Breslau NA, Weinreb JC, et al. Noninvasive localization of parathyroid adenomas: a comparison of x-ray computerized tomography, ultrasound, scintigraphy and MRI. *Magn Res Imaging* 1989;7:187–194.
22. Clark OH, Stark DD, Gooding GAW, et al. Localization procedures in patients requiring reoperation for hyperparathyroidism. *World J Surg* 1984;8:509–521.
23. O'Doherty MJ, Kettle AG, Wells P, Collins RE, Coakley AJ. Parathyroid imaging with technetium-99m-sestamibi: preoperative localization and tissue uptake studies. *J Nucl Med* 1992;33:313–318.
24. Taillefer R, Boucher Y, Potvin C, Lambert R. Detection and localization of parathyroid adenomas in patients with hyperparathyroidism using a single radionuclide imaging procedure with technetium-99m-sestamibi (double-phase study). *J Nucl Med* 1992;33: 1801–1807.
25. Neuman DR, Esselstyn Jr CB, MacIntyre WJ, et al. Primary hyperparathyroidism: preoperative parathyroid imaging with regional body FDG-PET. *Radiology* 1994;192: 509–512.
26. Melon P, Luxen A, Hamoir E, Meurisse M. Fluorine-18-fluorodeoxyglucose positron emission tomography for preoperative parathyroid imaging in primary hyperparathyroidism. *Eur J Nucl Med* 1995;22:556–558.
27. Sisson JC, Thompson NW, Ackerman RJ, Wahl RL. Use of F-18-fluoro-2-deoxy-d-glucose PET to locate parathyroid adenomas in primary hyperparathyroidism [Letter]. *Radiology* 1994;192:280.
28. Hellman P, Åkerström G, Juhlin C, Ridefelt P, Rastad J. Pathophysiology of hyperparathyroidism. In: Åkerström G, Rastad J, Juhlin C, eds. *Current controversy in parathyroid operation and reoperation.* Austin, TX: RG Landes Co.; 1994:9–22.
29. Juhlin C, Klareskog L, Nygren P, et al. Hyperparathyroidism is associated with reduced expression of a parathyroid calcium receptor mechanism defined by monoclonal antiparathyroid antibodies. *Endocrinology* 1988;122:2999–3001.
30. Juhlin C, Rastad J, Klareskog L, Grimelius L, Åkerström G. Parathyroid histology and cytology with monoclonal antibodies recognizing a calcium sensor of parathyroid cells. *Am J Pathol* 1989;135:321–328.
31. Sakaguchi K. Autocrine and paracrine functions of parathyroid tissue. In: Belizikian JP, Marcus R, Levine MA, eds. *The parathyroids. Basic and clinical concepts.* New York: Raven Press; 1994:93–106.
32. Wallfelt C, Ljunghall S, Bergström R, Rastad J, Åkerström G. Clinical characteristics and surgical treatment of sporadic primary hyperparathyroidism with emphasis on chief cell hyperplasia. *Surgery* 1990;107:13–19.
33. Lundgren E, Rastad J, Ridefelt P, Juhlin C, Åkerström G, Ljunghall S. Long-term effects of parathyroid operation on serum calcium and parathyroid hormone values in sporadic primary hyperparathyroidism. *Surgery* 1992;112:1123–1129.
34. Leskinen-Kallio S. Studies on the uptake of l-methyl-^{11}C-methionine in cancer with positron emission tomography. PhD thesis, University of Turku, Finland; 1992:8–54.
35. Ericson K, Lilja A, Bergström M, et al. Positron emission tomography with ^{11}C-methyl-l-methionine, ^{11}C-d-glucose and ^{68}Ga-EDTA in supratentorial tumors. *J Comput Assist Tomogr* 1985;9:683–689.
36. Bergström M, Muhr C, Lundberg PO, et al. Rapid decrease in amino acid metabolism in prolactin-secreting pituitary adenomas after bromocriptine treatment: a PET study. *J Comput Assist Tomogr* 1987;11:815–819.
37. Muhr C, Bergström M. Positron emission tomography applied in the study of pituitary adenomas. *J Endocrinol Invest* 1991;14:509–28.